Effect of fine and coarse recycled aggregates on high-temperature behaviour and residual properties of concrete

N. Algourdin, Prosper Pliya, A.L. Beaucour, A. Noumowé, D. Di Coste

Effect of fine and coarse recycled aggregates on high-temperature behaviour and residual properties of concrete

N. Algourdin[1,2*], P. Pliya[1], A.-L. Beaucour[1], A. Noumowé[1], D. di Coste[1]

[1] *CY Cergy Paris University, Laboratory of Mechanics and Materials of Civil Engineering (L2MGC), EA 4114, F-95000 Cergy-Pontoise, France*

[2] *University of Lyon, Laboratory of Tribology and Systems Dynamics (LTDS), UMR 5513, F-42023 Saint-Etienne, France*

[*] *Corresponding author:*

Email: nonna.algourdin@enise.fr

Tel: +33 (0)4 77 43 75 51

Abstract

This paper presents the results of an experimental study on the effect of recycled aggregates on concrete subjected to high temperatures. Concretes with natural aggregates (0S-0G), 30 % substitution of recycled concrete coarse aggregates and sand (30S-30G), and 100 % substitution of recycled gravel (0S-100G) were studied. The influence of recycled aggregates on the evolution of the thermophysical properties of concrete as a function of temperature when heated to 600 °C and then cooled, as well as on the temperature distribution within a cylindrical specimen was investigated. Thermal deformation measurements from 20 °C to 800 °C showed the favourable influence of the substitution of siliceous sand by recycled sand. For all concretes, residuals compressive strength and elastic modulus decrease and porosity increases with the temperature.

Keywords: *concrete, mortar, high temperature, recycled concrete aggregates, mechanical behaviour, thermal properties*

1. Introduction

Over recent years, the use of recycled aggregates in concrete has garnered significant attention from the scientific community. The production of concrete requires a significant amount of energy, which contributes heavily toward increasing the environmental impact of this process. Consequently, using quarry aggregates is environmentally unsustainable. Furthermore, recycling building waste is a major environmental issue. By contrast, reusing construction waste in the form of concrete aggregates could be beneficial for the environment because it can facilitate the preservation of natural resources and limit landfill pollution.

Recycled aggregates exhibit a higher absorption capacity and higher porosity, as compared with natural aggregates, owing to the presence of porous adhered mortar. Several researchers have studied recycled aggregate concretes (RACs) [1–5]. Further, certain testing recommendations have been proposed by international organisations [6,7]. Numerous mechanical tests on RACs have demonstrated a degradation in the mechanical properties owing to an increase in the percentage of recycled concrete aggregates (RCAs) [8–10]. Sami et al. [11] compared a natural aggregate concrete with two types of RACs: the first was cast and crushed in a laboratory, and the second was acquired from a dump site. They concluded that the compressive and splitting tensile strengths of the RACs were 10%–25% lower than those of conventional concrete. The reduction in the uniaxial tensile strength reached approximately 30%, whereas it was approximately 45% for the elastic modulus when the coarse aggregate of the concrete was completely replaced with RCAs [12]. Aggregates are the main constituents of concrete, and the modulus of elasticity of the concrete is largely determined by that of the aggregate. The lower failure strength of RACs can be explained by the lower crushing strength of the RCAs owing to the adhered mortar [13], as well as by the old interfacial transition zone (ITZ) between the original aggregate and the old paste, which constitutes an additional zone of weakness [14]. In addition, the presence of contaminants such as wood or asphalt may negatively affect the strength and elastic modulus of the RAC [15]. However, at a low level of replacement, up to 30%, no significant variations were observed in the mechanical properties.

Research into the impact of high temperatures on RCA properties remains in the nascent stages, and only a small amount of experimental data is available [16–20]. Yang et al. [21] studied the shear behaviour of 36 concrete beams with various percentages of substitution with RACs (0%, 50%, and 100%); the RAC samples were heated up to 20, 200, 300, and 400 °C. They concluded that the mechanical behaviour of the RAC at ambient temperature was minimally impacted by the RCA. Nevertheless, the residual shear strength and shear modulus declined rapidly with an increase in the temperature. Zega et al. [22] tested three types of RACs composed of RCA: granitic crushed stone, siliceous gravel, and quarzitic crushed stone; the RACs were heated up to 500 °C for 1 h. They noted

that the recycled concretes performed better than the corresponding conventional concretes. The RACs with quartzite aggregates exhibited the best performance. When exposed to fire, the material undergoes multiple alterations: aggregate expansion, shrinkage of the cement paste, increase in the vapour pressure within the material, or various thermal stresses that lead to concrete spalling [23,24]. Investigations on capillary water absorption, mercury porosity, and pore size distribution [25] indicated that concretes composed of 50% and 100% RCA exhibit less deterioration than with concretes composed of natural aggregates, following exposure to high temperatures (500 and 800 °C, respectively). In certain cases, a large amount of RCA yielded better results. Wang et al. [26] conducted residual tests for the compressive and splitting tensile strengths of concretes containing both coarse (100%) and fine RCAs (0%, 50%, and 100%). The target temperatures were 200, 400, 600, and 800 °C, with a heating rate of 12 °C/min. The concrete containing 100% RCA exhibited a higher normalised residual compressive strength than those containing 0% and 50% fine RCA. Laneyrie et al. [27] reported that the presence of non-cementitious contaminants had a larger negative impact on the deterioration of mechanical properties with temperature, as compared with the mechanical behaviour, at 20 °C.

Xuan et al. [28] demonstrated that using carbonated RCA (20% and 40%) could lead to better resistance under high temperatures (600 °C), as compared with granite aggregate conventional concrete. They noticed an improvement in the residual mechanical performance of the recycled concrete. Xie et al. [29] presented a method for improving the fire resistance of RCA by adding silica fume and steel fibres. The performance of the RCA was evaluated based on the residual compressive strength, elastic modulus, and toughness after heating at 200, 400, 600, and 800 °C. Water evaporation and hydrochemical decomposition were the main causes for the degradation of the RCA. However, the addition of steel fibres neutralised this negative impact.

Despite these previous studies, existing literature does not offer the results for the thermal deformation properties and thermal properties of RACs under “hot” conditions. These results are important for a better comprehension of the RCA behaviour at high temperatures. To address this deficiency in literature, in this study, the residual mechanical and physical properties of recycled concretes were examined. In addition, the evolution of heat transfer properties during heating, the analysis of thermal cracking and thermal expansion allows a better understanding of the impact of RCAs on the evolution of the residual properties as a function of temperature. Finally, quantifying the high temperature behaviour of RACs is fundamental to understand the fire performance of buildings made with recycled aggregates.

2. Experimental procedure

2.1 Raw materials

All the RCAs used in this study were provided by the French National Project PN RECYBETON [30] and conform with Eurocode 2 [31] C25/30 strength class (commonly used in the civil engineering domain).

Cement: Portland cement CEM II/A-L 42.5 N with a density of 3.09 kg/l, Blaine specific surface of 3590 cm^2 g^{-1} and compactness without superplasticizer of 0.548 was used in this study. The compressive strength measured in standard mortar at 28 days was 51.8 MPa.

Limestone filler: A filler of specific density 2.7 and Blaine surface 4620 $cm^2.g^{-1}$ was used to increase the granular skeleton of the mixture.

Aggregates: Natural crushed limestone coarse aggregates and recycled concrete coarse aggregates were used. The granular fractions of the natural gravel were 4/10 (NG1) and 6.3/20 (NG2). Recycled aggregates were produced by crushing the concrete waste from demolished buildings. The fractions of the RAC were 4/10 (RG1) and 10/20 (RG2). The original aggregate in the RCAs was alluvial gravel, which was mostly composed of flint (cryptocrystalline form of quartz mineral). Natural semi-crushed siliceous–calcareous sand (NS) and recycled concrete sand (RS) were used; both aggregates fraction were 0/4. Table 1 presents the physical properties of the aggregates, measured in accordance with the EN NF 1097-6 standard [32].

Table 1 Physical properties of aggregates

Aggregates	NG1	NG2	RG1	RG2	NS	RS
Granular fractions	4/10	6.3/20	4/10	10/20	0/4	0/4
Apparent density	2.71	2.71	2.29	2.26	2.59	2.08
Absorption, WA (%)	0.51	0.46	5.6	5.8	1.0	8.9
Moisture content before the mixing, W_0	1.4	1.3	12.8	13.1	2.1 – 2.59	15.2 – 19.4

** Wet aggregates were kept in a furnace at 80 °C until constant mass; moisture content was calculated as W_0 = (wet mass – dry mass) / dry mass × 100%*

Superplasticizer: A MC Power Flow 3140 superplasticizer was used. The density of the superplasticizer was 1.07, and the maximum alkali and chloride contents were 1.5% and 0.1%, respectively.

2.2 Mixtures and proportion design

Three types of concrete with an effective water/cement ratio of 0.67 were produced: 0S-0G (0% RCAs), 30S-30G (30% recycled gravel and 30% recycled sand by mass), and 0S-100G (100% recycled gravel and 0% recycled sand). These concrete mixtures were designed using the National French Project RECYBETON [30]. Table 2 lists the mix proportions of these concretes. The total volume RCA fraction of the 30S-30G mix was 53.0% and that of the 0S-100G mix was 55.1%. The RCA was pre-saturated to 1% (absolute value) above its absorption coefficient in barrels 48 h before mixing with water content of: 9.9 % for ***RS 0/4, 6.6 % for **RG 4/10, 6.8 for RG 10/20.

Table 2 Mix proportions of concretes for dry aggregates

	Concretes	0S-0G	30S-30G	0S-100G
Mixture proportions (kg/m^3)	**Cement**	270	277	282
	Limestone filler	45	31	31
	Effective water	180	185	189
	Total water	192.93	230.62	246.85
	Superplasticizer (dry extract)	1.15	1.12	1.40
	NG* 4/10	267	171	0
	RG 4/10**	0	145	163
	RG 4/10 (vol %)	0.0	14.90	10.3
	NG 6.3/20	820	552	0
	RG 10/20	0.0	167	701
	RG 10/20 (vol %)	0.0	10.5	44.8
	NS* 0/4**	780	500	806
	RS 0/4	0	218	0
	RS** (vol %)**	0.0	27.6	0.0
Slump, (cm)		19	21	16

Compression strength (MPa) (described in 2.5.1)	$f_{c\ 28\ days}$	40.0 ± 1.4	38.7 ± 1.4	31.8 ± 1.1

*NG - natural gravel; **RG - recycled gravel; ***NS - natural sand; ****RS - recycled sand.

The *effective water* is defined as the amount of free water available to react with the cement of the mixture and for workability. The *total water* is the overall amount of water in the mixture including the water absorbed by aggregates. So the porosity and strength of concretes depends on the effective water/cement ratio which doesn't varies between the mixtures. The volume fractions of fine (NS) and coarse aggregate (NG) are calculated according to the compressible packing model to optimize the granular skeleton compactness to minimize the water demand of the mixture [33]. For 30S-30G concrete, 30% mass fraction of fine aggregate related to overall fine aggregate is substituted by recycled fine aggregate (RS) and 30% mass fraction of coarse aggregate related to overall coarse aggregate is substituted by recycled coarse aggregate (RG). The slump test was carried out using a steel mould known as Abram's cone. The slump of the concrete was determined by measuring the distance from the top of the slumped concrete to the level of the top of the slump cone.

The concrete mixer of 25 litres was used to prepare the samples. The mixing sequence was: first, introduction of gravel, half of the sand, cement, limestone filler and the other half of the sand, than mixing for 1 minute. Second, introduction of the added water incorporating the adjuvants and mixing for 0.5 minutes. Third, continued mixing for 3.5 minutes.

Considering a relatively small size of the samples ($\varnothing$ < 16 mm and length > 20 mm), imposed by the dilatometer device, a thermal expansion study was conducted on the mortar mixes, rather than the concretes. Therefore, the geometry of the specimens can be considered as representative of the raw material.

Four mortar mixtures were produced based on the mix proportions of the 0S-0G concrete. The objective was to remove the fraction of coarse aggregates, while keeping all the other proportions constant. However, the amount of water was reduced because the initial quantity led to greater fluidity and caused segregation. Consequently, the water/binder ratio changed from 0.48 to 0.4. Four mixes were manufactured using various percentages of substitution with recycled sand: 0S (100% natural sand or 0% recycled sand), 30S (30% recycled sand), 70S (70% recycled sand), and 100S (100% recycled sand) (Table 3). The volume of aggregates is the same for the three formulations. The water and cement volumes are slightly different to adjust the same strength class.

Table 3 Mixture proportions of mortars

Mixture proportions (kg/m^3)	Mortars	0S	30S	70S	100S
	Cement	300	300	300	300
	Effective water	88.4	88.1	88.9	88.9
	Superplasticizer	5.41	6.4	3.8	3.8
	NS 0/4	2136	1495	641	0
	RS 0/4	0	614	1434	2048

2.3 Curing conditions

Concrete cylindrical specimens with dimensions of 150 mm × 300 mm and mortar prismatic specimens with dimensions of 40 × 40 × 160 mm were cast. The specimens were retained in their moulds for 24 h. Based on RILEM recommendations, they were removed from their moulds and kept in plastic bags with wet rags to avoid water evaporation until the day of the test [34]. The specimens were maintained at room temperature (19 °C ± 3 °C). They were cured for at least 90 days to ensure that the pozzolanic reactions were stabilised and that there was limited interstitial water in the concrete.

2.4 Heating–cooling methodology

Heating tests were performed in an electric Ceradel furnace (Figure 1) with dimensions of 1300 × 1010 × 1040 mm, along with a ventilation system to homogenise the temperature within the furnace.

Figure 1 Exterior of electric furnace

Type-K thermocouples connected to an automatic data acquisition device were used to monitor the temperatures in the furnace room and on concrete surface at intervals of 30 s. The temperature at the surface of the concrete controls the increase of temperature in the furnace. A metal grid was placed in the oven to protect the heating resistances from damage, in the event of spalling.

Three heating–cooling cycles were performed for the concretes. The specimens were subjected to temperatures ranging from room temperature to 300, 450, and 600 °C. Each cycle included an increase in temperature at the rate of 0.5 °C/min, a 2 h temperature dwell, and a cooling stage at the rate of 0.5 °C/min. The low heating rate ensured the homogeneity of temperature and limited the thermal gradient in the specimen during the heating and cooling stages.

2.5 Tests

Table 4 Specimens (type and size) and heating–cooling temperatures corresponding to each test

Tests	Type and number of specimens, mm	Heating conditions (°C)
Porosity (four specimens per mix)	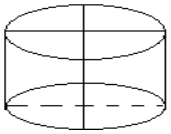 ¼ of sample; 150 (Ø) × 50	80 °C, 300 °C, 450 °C, 600 °C
Statistical cracking analysis (two specimens per mix)	 160 (Ø) × 50	300 °C, 450 °C, 600 °C
Thermal properties: conductivity, specific heat, diffusivity (three specimens per mix × two slices)	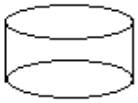 110 (Ø) × 40	From 30 °C to 600 °C, 30 °C

Thermal response (2–3 specimens per mix)	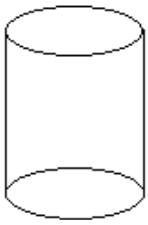 150 (Ø) × 300	600 °C Heating rate: 0.5 °C/min
Compressive strength (f_c) (four specimens per mix)	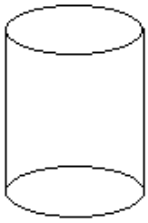 150 (Ø) × 300	300 °C, 450 °C, 600 °C
Dynamic elastic modulus (E_{dyn}) (four specimens per mix)	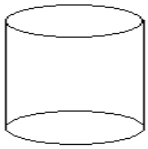 150 (Ø) × 100	300 °C, 450 °C, 600 °C
Dilatometry (three specimens per mix)	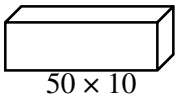 50 × 10	20–1000 °C (heating) and 1000–210 °C (cooling) at the rate of 10 °C/min

The change in the concrete microstructure was evaluated based on analyses of the total water porosity and cracking. The heat transfer during heating and cooling was analysed considering the thermal conductivity, thermal diffusivity, specific heat, and thermal response. Furthermore, investigations on the compressive strength and dynamic modulus of elasticity and dilatometry were performed. All the tests, including those for determining the type of specimen and heating–cooling cycles, are summarised in Table 4.

2.5.1 Measurement of residual properties

Water-accessible porosity: The water porosity (n) of the concretes was examined based on the NF P 18-459 standard [35]. Four concrete samples were used for each temperature and concrete mix (Table 4). The specimens were placed in an oven at 80 °C until they reached a constant mass or heated at 300 °C, 450 °C, or 600 °C. The oven-dried/heated samples were placed in a vacuum to eliminate the air from the internal pores. Water was then introduced into the vacuum vessel to soak the samples for 44

h (Figure 2). Degassing of the water was necessary to ensure the maintenance of a vacuum during the connection between the vacuum bell containing the samples and a water bottle. The weights were measured immediately after disconnecting the pump.

Figure 2 Porosity measurement setup

The volume of the voids was deduced based on the difference in mass between the saturated-surface dry mass (M_{sat}) and the oven-dry mass (M_{dry}). The dry mass of the concrete (M_{dry}) was obtained at the end of the heating cycle. The apparent volume of aggregates was measured by hydrostatic weighing of the saturated aggregate (M_{hydr}). The porosity (n), presented as a percentage of volume, is expressed as follows:

$$n = (M_{sat} - M_{dry}) \times \rho_{water} \times 100 / (M_{sat} - M_{hydr})$$

Evolution of crack network: Crack mapping was carried out on the surface of 50-mm-thick slices; these slices were cut from a 150 × 300 mm cylinder of the recycled and natural concretes before heating.

Furthermore, AutoCAD software was used to perform statistical analyses for different heating cycles. The specimen's cracks were reported on tracing paper for each mix heated up to 450 °C and 600 °C, digitised and used to obtain quantitative results for crack evolution.

Compressive strength (f_c): For each mix and heating–cooling cycle, four 150 × 300 mm cylinders were tested for compressive failure after surface smoothing using sulphur. The tests were conducted at room temperature following the heating–cooling cycles, using a 3000-kN INSTRON hydraulic press. The concrete specimens were tested for uniaxial compressive loading at an imposed stress rate of 0.5 MPa.s^{-1}, based on the European standard EN 12390-3 [36].

Dynamic elastic modulus (E_{dyn}): The dynamic Young's modulus was measured using an ultrasonic wave propagation test device from Pundit Lab, based on EN 12504-4 [37]. The device emits an electric signal through the specimen, which is then converted into waves by a piezoelectric transducer. Petroleum jelly was used to ensure perfect contact between the face of each transducer and the concrete sample. The wave propagates in the sample from one transducer to the other and is then reflected to the first transducer. The apparatus measures the time t between two successive echoes,

based on which the longitudinal ultrasonic wave speed can be calculated as $V = L/t$, where V is the ultrasonic wave speed [in m/s], L is the length of the cross-piece material [in m], and t is the time required for wave propagation along length L [in µs].

The dynamic Young's modulus was calculated using the following relationship: E [in GPa] = $\rho(V^2(1 + U)(1 - 2U))/(1 - U)$, where V is the ultrasonic wave speed [in m/s], ρ is the concrete density [in kg/m^3] measured after each heating cycle, and U is Poisson's ratio (considered as 0.2 for concrete).

2.5.2 Thermo-physical and thermo-mechanical behaviour

Thermal properties: The thermal properties evaluated include the thermal conductivity λ, thermal diffusivity a, and heat capacity (C_p). These properties were measured during the heating cycle up to 600 °C and then during the cooling cycle, by using a hot-disc probe TPS1500 based on the method developed by Gustaffson ([38], [39]) and transient plane source technology. The specific heat was calculated using the conductivity and diffusivity measurements. A mica probe with a radius of 14.61 mm and a very fine nickel double spiral (with thickness of 10 µm) covered with two thin layers of electrically insulating materials was placed between the two symmetrical halves of the concrete cylinder slices (diameter 110 mm × height 40 mm). Each sample had a flat surface to prevent contact defects with the sensor.

The cylinder slices were pre-dried at 80 °C until a constant mass was obtained and thereafter heated in a 5 L electric oven controlled using Hot Disk. The heating rate was 1 °C/min, and the measurements were conducted under isothermal conditions of 30, 150, 200, 250, 300, 450, 500, 550, and 600 °C. Three measurements were performed for each temperature and sample.

Thermal response: A study on the thermal response was carried out by measuring the temperatures, up to 600 °C, at the surface, quarter diameter (Ø/4), and centre (Ø/2) of the specimens (Figure 3). Three 150 × 300 mm specimens per mix were equipped with the type-K thermocouples. A heating rate of 0.5 °C/min was employed.

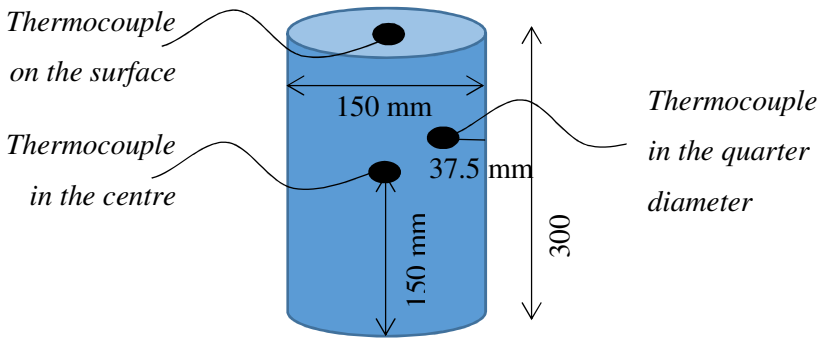

Figure 3 Placement of thermocouples in 150 x 300 mm specimens

Dilatometry (dl/l_0): The expansion of the mortar specimens was measured on a DIL 402 PC (NETZSCH) device (Figure 4). The specimens (50 mm × 10 mm) were heated up to 1000 °C at a heating rate of 10 °C/min. Each specimen was pressed against the bottom of the sample holder with a force of 25 N. The pushrod was directly connected to the displacement transducer, which was locked in an inert environment to improve device precision. A specimen thermocouple was then placed to coordinate the expansion measurements with the furnace temperature.

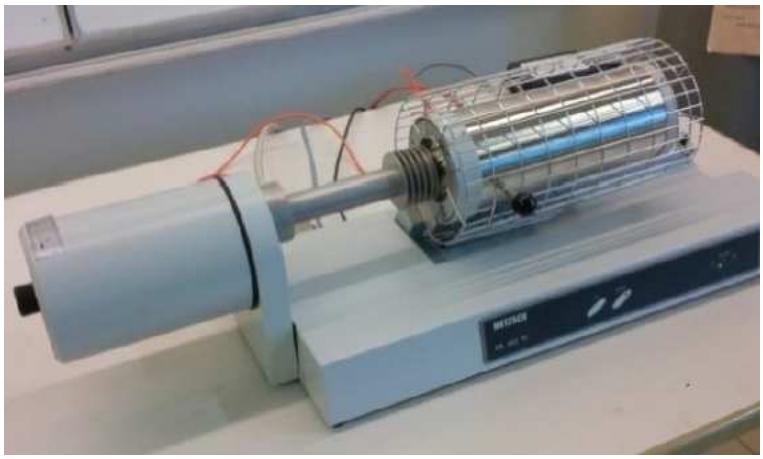

Figure 4 DIL 402 PC device

3. Results and discussion

3.1 Thermal properties

Table 5 summarises the thermal properties at room temperature. In most cases, the standard deviation was low (between 0.0009 and 0.01) and not noticeable on the graphs (Figure 5, Figure 6, and Figure 7).

The RACs exhibited lower thermal conductivities than the natural aggregate concrete. This observation is consistent with the higher values of total porosity (see Section 3.2.1). The conductivities of the three concretes decreased with an increase in the porosity. However, there were no significant

differences in the diffusivity results. The small increase in the specific heat was counterbalanced by the decrease in the density.

Table 5 Thermal properties at ambient temperature

Properties	0S-0G	30S-30G	0S-100G
Thermal conductivity ($W.m^{-1}.K^{-1}$)	2.10 ± 0.02	1.73 ± 0.04	1.61 ± 0.17
Specific heat ($kJ.kg^{-1}.K^{-1}$)	1.05 ± 0.1	1.09 ± 0.1	1.12 ± 0.1
Thermal diffusivity ($mm^2.S^{-1}$)	0.70 ± 0.02	0.74 ± 0.04	0.68 ± 0.05

3.1.1 Thermal conductivity

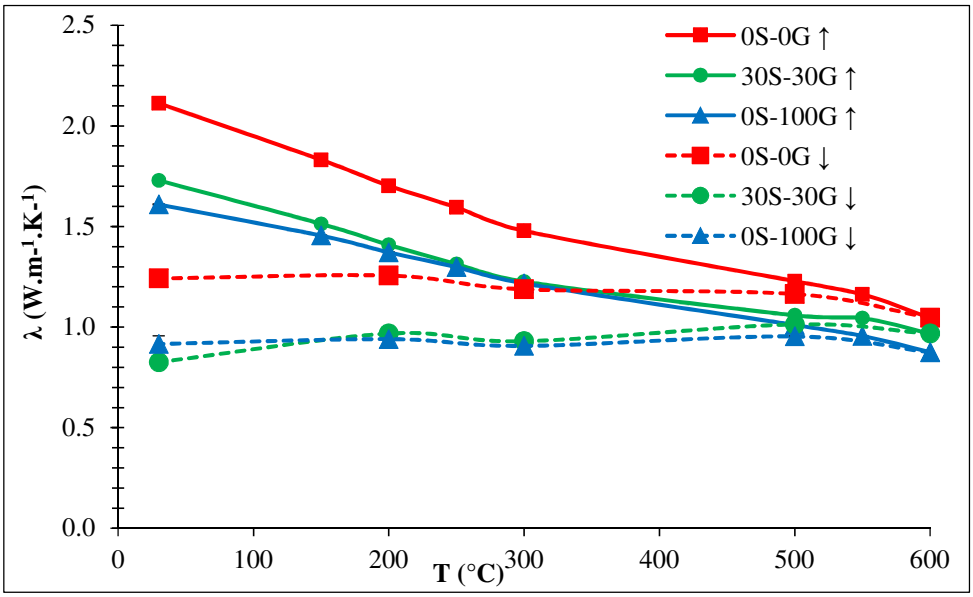

Figure 5 depicts the trends in the evolution of the thermal conductivities (λ) of the 0S-0G, 30S-30G, and 0S-100G concretes as functions of the temperature during heating and cooling. At 30 °C, the thermal conductivities of the RACs (30S-30G and 0S-100G) were lower than that of plain concrete (Table 5). Thermal conductivity is dependent on various parameters, such as the volume, pore distribution, and mineralogy of the aggregate components. Natural limestone aggregates were used for the 0S-0G concrete, whereas the recycled concretes were mostly composed of flint. Both aggregates exhibit similar thermal conductivities [40]. The substitution of natural limestone aggregates with the

Figure 5 Evolution of thermal conductivity of concretes during heating (↑) and cooling (↓)

recycled aggregates essentially involves an increase in the porosity and volume fraction of the cement paste, as compared with those of the aggregates. A low air conductivity (0.026 W/m.K) and cement conductivity could explain the low conductivities of the 30S-30G and 100-0R concretes.

At elevated temperatures, the thermal conductivity of all the concretes decreased to 600 °C. This decrease was partly related to the increase in the vibrational energy of the crystal lattice (phonons), which increased the number of collisions between phonons, thereby increasing the resistance to the flow of heat [27]. The more significant the scattering, the lower is the conductivity. Moreover, physicochemical transformations and microcracking caused by the thermal constraints reduce the conductive connections and generate an additional volume of pores [41].

The thermal conductivities progressed almost linearly from 30 to 600 °C. It was noted that the thermal conductivity of the 0S-0G concrete decreased more rapidly than those of the 30S-30G and 0S-100G concretes. Thus, the difference between the natural aggregate and RACs decreased with increasing temperature. It is typically observed that the most conductive concretes exhibit a faster loss of thermal conductivity with an increase in temperature ([42], [43], and [44]). The average loss in thermal conductivity for a temperature increase of 100 °C was 0.17 W/m.s for the 0S-0G concrete and 0.13 and 0.12 W/m.s for the 0S-100G and 30S-30G concretes, respectively. The thermal conductivity of the 0S-0G concrete at 600 °C represented 50% of its initial value, against 55% for the two other concretes (30S-30G and 0S-100G). These values were similar and within the range of values reported in literature for most concretes.

Thermal conductivity measurements during the cooling phase demonstrated hysteresis, which indicates the irreversibility of the reaction, leading to the deterioration of the material as well as the departure of the physically and chemically bound water and the appearance of microcracks ([45] and [44]).

3.1.2 Specific heat

Figure 6 presents the trends in the evolution of the specific heats of the 0S-0G, 30S-30G, and 0S-100G concretes as functions of the temperature during heating and cooling. At 30 °C, the recycled aggregate and plain concretes exhibit similar specific heat values. Hence, the effect of the recycled aggregates on this thermal property was not significant.

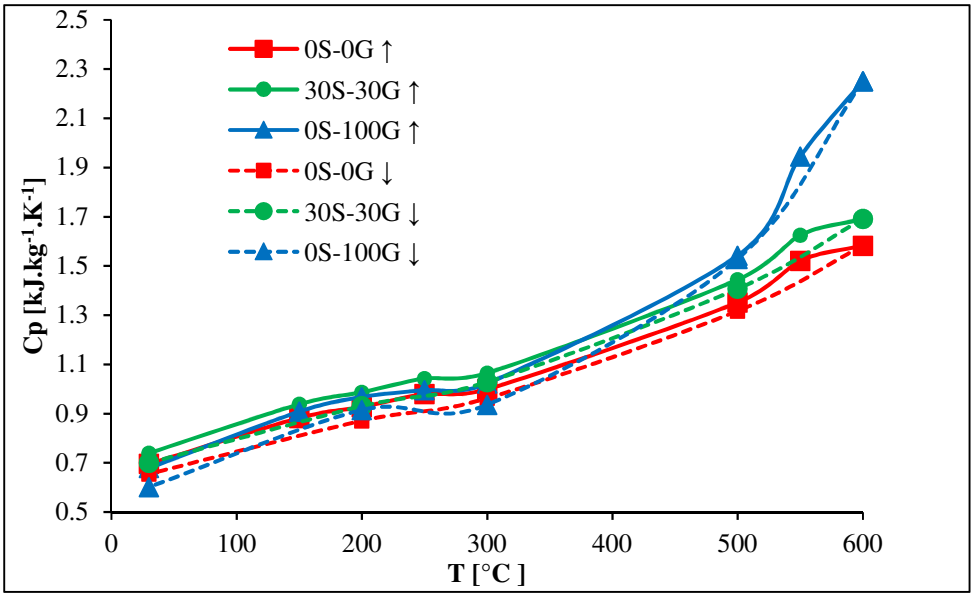

Figure 6 Evolution of specific heat during heating (↑) and cooling (↓)

The results indicate an increase in the specific heat with the temperature. This increase was particularly observed between 30 and 150 °C and between 500 and 600 °C. These exact specific heat evolutions could also be observed for other concrete types with or without fibres [44]. The trends in the evolution of the specific heat for the three concretes were similar up to 500 °C. Beyond 500 °C, however, the specific heat of the 0S-100G concrete exhibited a drastic surge. The hysteresis phenomenon was less notable than that in the case of thermal conductivity. The increase in thermal capacity with temperature is mostly related to the reversible phenomena. The specific heat is strongly dependent on the atomic vibration, which is the main absorption mode for thermal energy in solids. The amplitude of the vibrations increases with temperature, leading to higher values of the specific heat. It is essential to note that there exists a significant difference between the measured value at 600 °C during heating and the residual value after cooling.

3.1.3 Thermal diffusivity

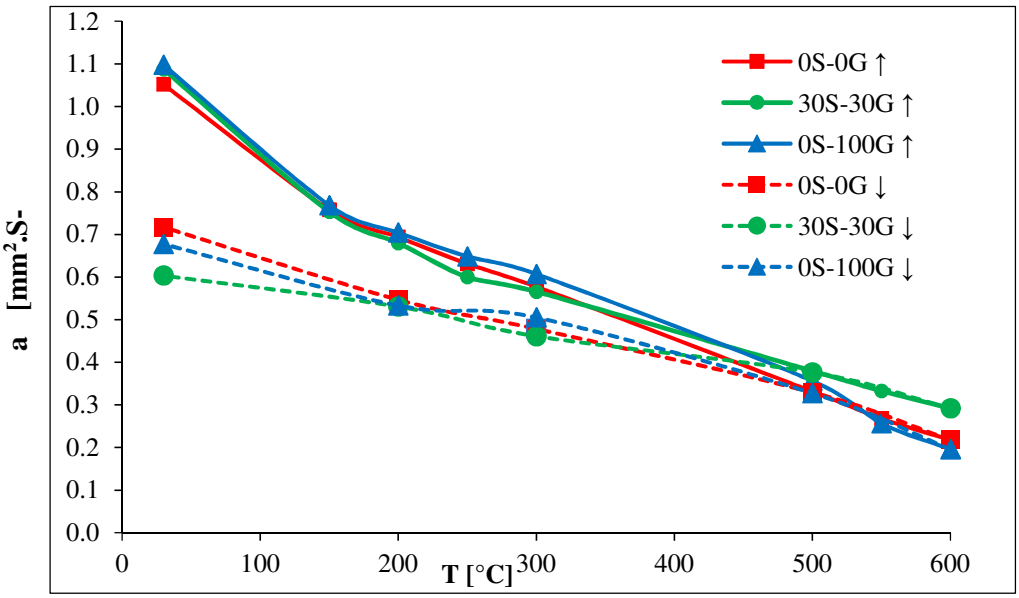

Figure 7 Evolution of thermal diffusivity during heating (↑) and cooling (↓)

The trends in the evolution of thermal diffusivity ($a = \lambda/(C_p \times \rho)$) are presented in Figure 7. As can be seen, thermal diffusivity decreases gradually with temperature. The previous results indicated that a decrease in conductivity was followed by an increase in the volume thermal capacity. This explains the decrease in the thermal diffusivity during heating. The relative loss of diffusivity with an increase in temperature was greater than that in conductivity. Thus, the values at 600 °C represent only approximately 20% of the values at room temperature. The results obtained for the three concretes (0S-0G, 30S-30G, and 0S-100G) were similar.

3.1.4 Effect of recycled aggregates on thermal response of specimens

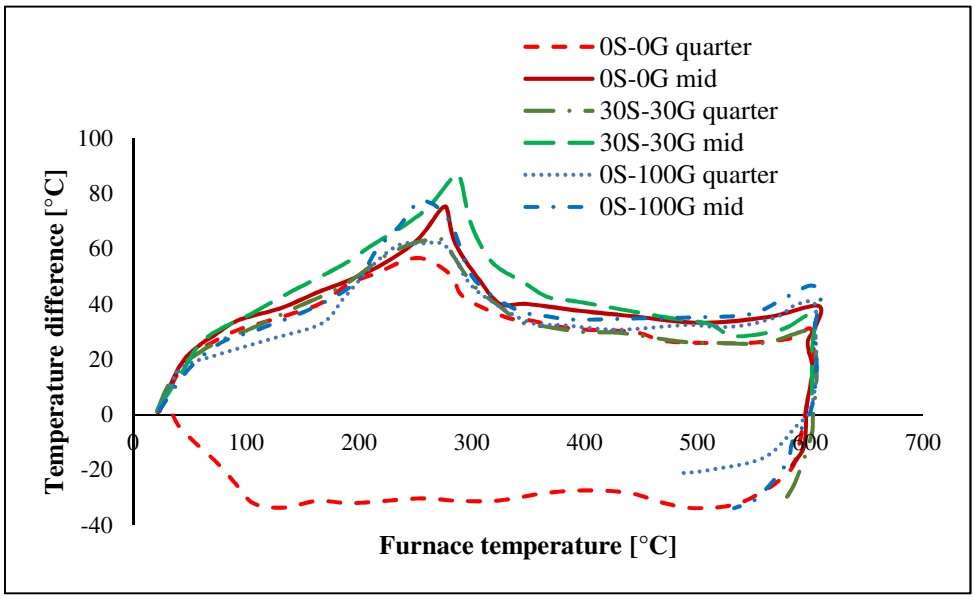

Figure 8 Evolution of temperature difference between the surface and centre (mid) and between the surface and quarter (quarter) of 150 mm × 300 mm concrete cylinders as a function of surface temperature during heating–cooling cycles

Figure 8 presents the temperature difference between the surface and the centre (or quarter) of the specimens for the 0S-0G, 30S-30G, and 0S-100G concretes during the heating–cooling cycles up to 600 °C. The thermograms at both depth measurements (centre and quarter) indicated similar trends in evolution. The maximum temperature difference was noted at a surface temperature of 240–255 °C for the quarter diameter of the specimen and at 260–280 °C for the centre measurement. A slightly lower temperature peak was observed for the 0S-0G concrete, as compared with the recycled concretes. This peak could be attributed to the latent heat consumption associated with hydrate decomposition and water evaporation. The slightly greater temperature difference for the RACs could be attributed to the high level of absorption of the aggregates.

The recycled aggregates and cement paste volumes of the 30S-30G and 0S-100G concretes were almost identical. The more significant peak observed for the 30S-30G concrete may be related to the high absorption coefficient of the recycled sand, as compared with that of the recycled gravel; this consequently led to the higher free water content. It is essential to note that the aggregates were saturated before casting.

The second increase in the temperature difference between the two RACs (30S-30G and 0S-100G) was observed at approximately 600 °C. This temperature gradient was associated with the deshydroxylation of portlandite. This new increase was more evident for the 0S-100G and 30S-30G

concretes than for 0S-0G concretes, which can be explained by the additional cement paste provided by the recycled aggregates.

3.2 Evolution of concrete microstructure

3.2.1 Evolution of water porosity

Figure 9 depicts the trends in the evolution of the absolute porosities of the 0S-0G, 30S-30G, and 0S-100G concretes as functions of the temperature. After drying at 80 °C, the porosity increased with the quantity of RCA. At this temperature, the porosities were 12.9% ± 0.5%, 14.7% ± 0.5%, and 17.3% ± 0.4% for the 0S-0G, 30S-30G, and 0S-100G concretes, respectively. All the concretes featured almost the same volume of aggregates. Therefore, the higher porosity of the RAC could be attributed to the porosity of the recycled aggregates and the excess mortar of the RCA. This finding has been reported in previous studies [27,46,47].

After each heating–cooling cycle, an increase in porosity was observed at 300 °C. The increase in porosity was 18%, 29%, and 18% (percentage difference compared to that at 80 °C) at 300 °C and 46%, 42%, and 32% at 600 °C for the 0S-0G, 30S-30G, and 0S-100G concretes, respectively.

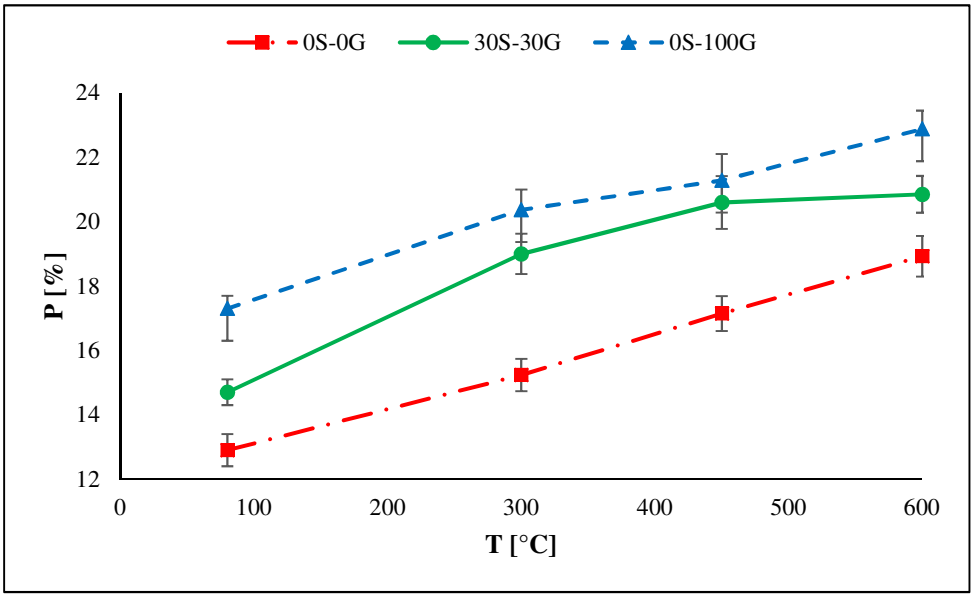

Figure 9 Evolution of residual absolute porosities for 0S-0G, 30S-30G, and 0S-100G concretes as functions of temperature

From 80 to 450 °C, the porosity of the 30S-30G concrete increased more rapidly than that of the 0S-100G concrete. At 450 °C, the difference in water porosity between the two RACs was 0.7%. Beyond 450 °C, the porosity of the 30S-30G concrete remained almost constant, whereas that of the 0S-100G concrete continued to increase. As compared with the other concretes, the 0S-100G concrete exhibited a slightly higher increase in porosity during heating. This is consistent with the overall increase in the number of cracks in the concrete, as described in Section 3.2.2.

The water porosity increases with the increasing of recycled aggregates and it is attributed to the presence of the multiple ITZs.

3.2.2 Statistical cracking analysis

Table 6 presents the typical crack patterns that appear on the surfaces of the specimens following the 450 and 600 °C heating–cooling cycles. Heating the specimens up to 300 °C leads to the formation of a few minor macrocracks in the concrete specimens. The specimens heated to 150 or 300 °C are not presented in Table 6, because the minor cracks in these specimens could not be observed with the naked eye.

Beyond 300 °C, a few visible cracks appeared on the surfaces of the recycled concrete specimens, located mainly at the interfacial transition zones (ITZs) of the paste/natural aggregate and the old paste/new paste [27,46,48]. Spalling and reddening of a portion of the original flint aggregates were observed within the recycled aggregate. As depicted in Figure 10, the 0S-100G concrete specimens exhibited the melting of waste in the form of bitumen.

Figure 10 Surface of 0S-100G concrete after heating–cooling up to 300 °C

Upon heating up to 450 °C, very few cracks appeared on the surface of the 0S-0G concrete. By contrast, the 30S-30G and 0S-100G concrete specimens presented visible cracks; these mostly appeared at the interface of the old paste/aggregates. In the case of the 0S-100G concrete, trans-granular cracks appeared in the flint aggregates. This could be attributed to the unstable nature of the flint aggregates, which undergo spalling between 150 and 450 °C, as described in a previous report [49]. Furthermore, tangential and radial cracks appeared near the large aggregates in the 0S-100G concrete.

Heating up to 600 °C led to an increase in the number of cracks and their lengths. The 0S-0G concrete exhibited crack initiation, with the cracks spreading between the aggregates and cement paste. The reddening and bleaching of the aggregates were accelerated, and the cracks spread throughout the grain. These phenomena were also observed by Razafinjato [40]. The reddening of the flint aggregates is a common phenomenon that occurs with an increase in temperature. The limestone aggregates exhibited surface cracking, whereas the flint aggregates featured cracks perpendicular to the surface of the grain, which appeared to spread deeply within the grain. The calcareous aggregates of the 0S-0G concrete exhibited more surface tangential than surface radial cracks, as compared with the RAC.

Table 6 Crack patterns on surfaces of 0S-0G, 30S-30G, and 0S-100G concretes following heating–cooling at 450 and 600 °C.

	0S-0G	30S-30G	0S-100G
450 °C	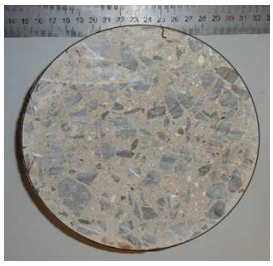		
	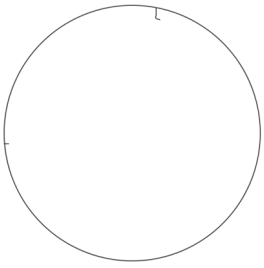	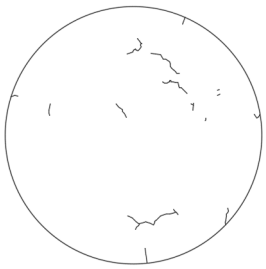	

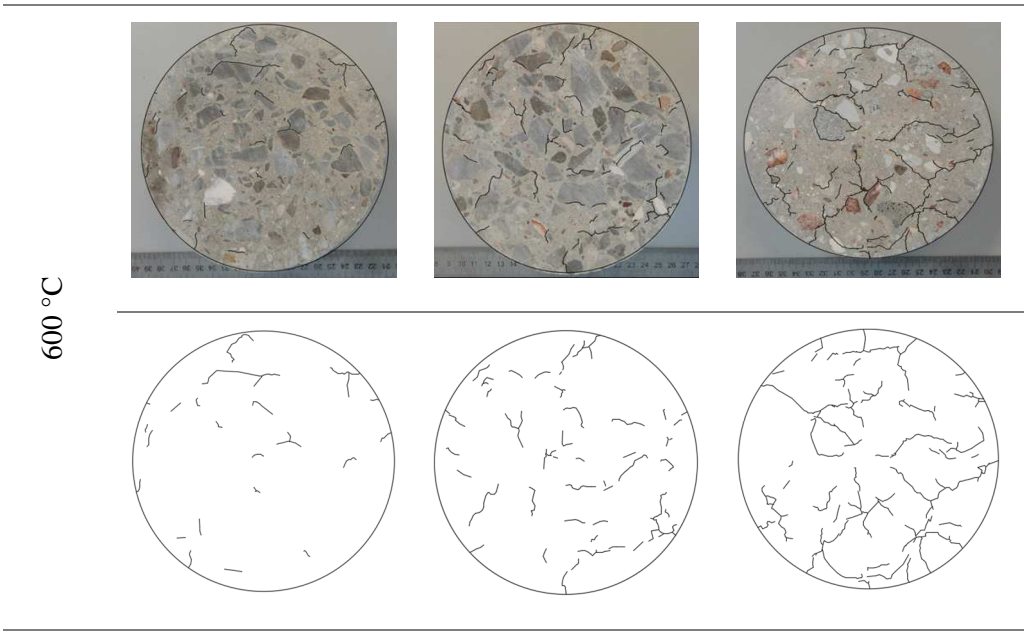

Table 7 presents the statistical analysis of the cracks observed on the surface of each recycled concrete following the heating at 450 and 600 °C. The width of the cracks was no larger than 1 mm.

Table 7 Analysis of cracks on surfaces of each recycled concrete following heating at 450 and 600 °C

Cumulative visible crack length [mm]						
	0S-0G		**30S-30G**		**0S-100G**	
	Specimen 1	**Specimen 2**	**Specimen 1**	**Specimen 2**	**Specimen 1**	**Specimen 2**
450 °C	2	12	172	98	680	912
600 °C	288	410	617	705	1213	1187

In general, it was noted that the natural aggregate concrete specimens exhibited less cracks and shorter crack lengths than the RAC specimens. Beyond 450 °C, the crack lengths for the 0S-100G concretes were almost three times that for the 0S-0G concretes. The difference in the crack lengths between the 0S-100G and 30S-30G concretes was more remarkable at 450 °C than at 600 °C (Figure 11).

The cracking surfaces indicated that the cracks were mostly widely distributed and intergranular in the recycled coarse aggregates, which were primarily composed of flint. The flint aggregates exhibited significantly greater thermal expansion than the limestone aggregates at 400 °C [40]. The stresses generated by the thermal deformation incompatibilities between the cement paste and the surface increased with the size of the aggregates. The differences in dilatation were higher in terms of the absolute values because of the large aggregate sizes. The paste/aggregate bond resistance decreased

with the size of the aggregate. Notably, the transition aureole (ITZ) around the aggregates increased with the aggregate size.

The 30S-30G and 0S-100G concretes contain the same total volume fraction of recycled aggregates, as determined via the Dreux-Gorisse method [50]; however, the 0S-100G concrete contains a larger weight of recycled coarse aggregates.

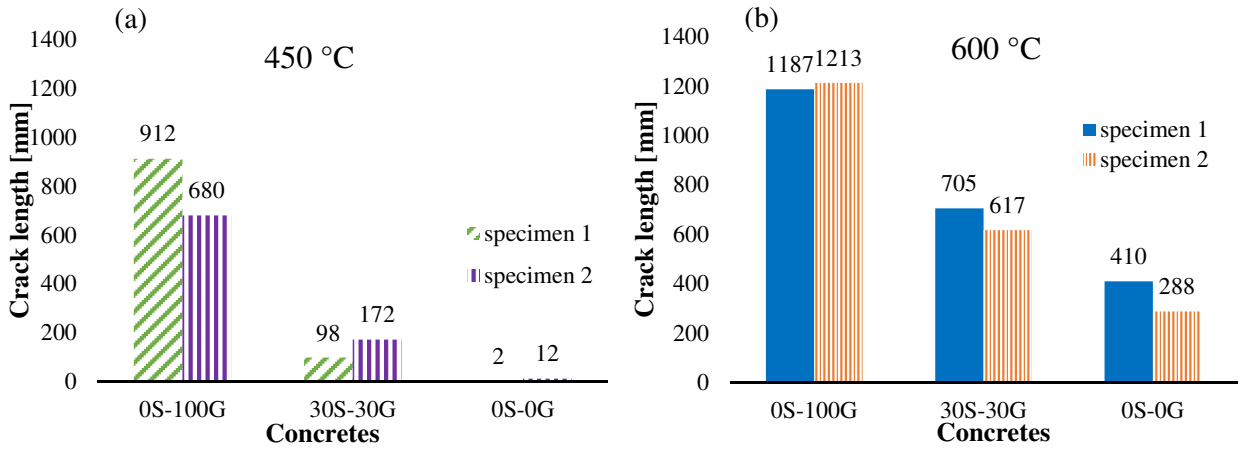

Figure 11 Cumulative length of cracks for 0S-0G, 30S-30G, and 0S-100G concretes at (a) 450 °C and (b) 600 °C

3.3 Residual mechanical properties

Mechanical tests were conducted after cooling for evaluating the impact of the recycled aggregate content on the concrete strength. Table 8 summarises the results for the compressive strength (R_c) and dynamic modulus of elasticity (E) before and after each heating–cooling cycle.

At 20°C, the compressive strength of 0S-0G is higher than that of 30S-30G and 0S-100G concretes. On the contrary, the 30S-30G presents higher elasticity modulus than that of 0S-0G and 0S-100G concretes. It could be due to the rehydration of the old cement, which is mainly present in recycled sand.

Table 8 Compressive strength and dynamic modulus of elasticity.

Concretes	Tests	20 °C	300 °C	450 °C	600 °C
0S-0G	f_c (MPa)	40.0 ± 1.4	22.6 ± 1.1	18.4 ± 1.8	11.4 ± 1.2
	E (GPa)	31.5 ± 0.3	26.4 ± 0.3	12.1 ± 0.1	7.2 ± 0.2

30S-30G	f_c (MPa)	38.7 ± 1.4	32.9 ± 2.6	21.3 ± 1.2	13.0 ± 1.2
	E (GPa)	35.6 ± 1.5	24.3 ± 1.1	14.0 ± 0.1	5.7 ± 0.1
0S-100G	f_c (MPa)	31.8 ± 1.1	30.2 ± 0.7	15.4 ± 0.9	8.6 ± 0.5
	E (GPa)	29.5 ± 0.4	17.3 ± 0.2	9.1 ± 0.1	4.0 ± 0.0

3.3.1 Residual compressive strength

The evolutions of the relative residual compressive strengths of the 0S-0G, 30S-30G, and 0S-100G concretes are depicted in Figure 12. The relative residual strength (modulus) was calculated by dividing the residual strength (modulus) after the heating–cooling cycles (f_c, E) with the results for the unheated concretes (f_{c20}, E_{20}). The residual compressive strength of the 0S-0G concrete decreased gradually from 20 to 600 °C, whereas the residual compressive strength of the 30S-30G and 0S-100G concretes decreased significantly after 300 °C. These results are consistent with the observations of the crack network (Section 3.2.2). The thermal strain mismatch [51] between the aggregate and paste is more significant in the RAC.

The relative residual strengths of the 0S-0G and 30S-30G concretes were considerably similar between 20 and 300 °C (f_c/f_{20} = 83%–85%). The relative residual strength of the 0S-100G concrete was higher than that of the other two concretes up to 300 °C. Beyond 300 °C, the relative residual compressive strength of the 0S-100G concrete decreased more drastically than that of the 0S-0G and 30S-30G concretes. Over the entire heating period, a negative impact of 100% substitution with recycled gravel was observed. The RACs (30S-30G and 0S-100G) indicated a higher percentage of decrease in strength beyond 300 °C. The 30S-30G concrete indicated a weak impact of recycled aggregates on the evolution of its compressive strength.

The increase in RCA leads to a decrease of the compressive strength. The lower mechanical quality of RCA, compared to natural aggregates, explains this performance reduction. Natural aggregates are produced from rocks with the compressive strength exceeding 50 MPa, whereas the RCA are obtained by concrete crashing with lower compressive strength.

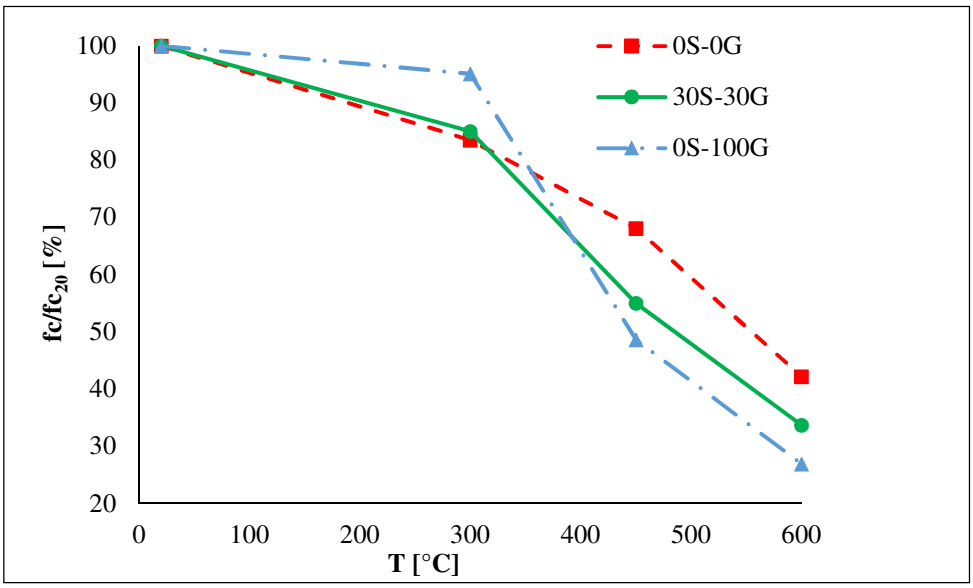

Figure 12 Relative residual compressive strengths of 0S-0G, 30S-30G, and 0S-100G concretes as functions of temperature

3.3.2 Residual dynamic modulus of elasticity

Figure 13 depicts the evolutions of the relative residual (after heating–cooling period) dynamic modulus of elasticity for the 0S-0G, 30S-30G, and 0S-100G concretes as functions of temperature. At 20 °C, the values of the dynamic modulus of elasticity for the 0S-0G and 0S-100G concretes were similar ($E_{0S\text{-}0G}$ = 31.5 GPa, $E_{30S\text{-}30G}$ = 35.6 GPa, and $E_{0S\text{-}100G}$ = 29.5 GPa). Beyond 300 °C, the residual modulus of elasticity of the 0S-0G concrete decreased gradually, whereas the decrease in the residual modulus of elasticity of the RACs was more drastic. This behaviour of the concretes was consistent with the development of cracks (Section 3.2.2). The high cracking density of the RACs could increase their porosities, which would significantly decrease their residual moduli of elasticity. Beyond 600 °C, the three concretes indicated similar values for these moduli ($E_{0S\text{-}0G}$ = 7.2 GPa, $E_{30S\text{-}30G}$ = 5.7 GPa, and $E_{0S\text{-}100G}$ = 4.0 GPa). The replacement of natural aggregates with recycled coarse aggregates did not significantly alter the trend of the curve beyond 300 °C.

The degradation in the modulus of elasticity was more rapid, as compared with that in the residual compressive strength. Furthermore, relative to the two other concretes (average value of 82%), the 0S-100G concrete exhibited a greater loss in the residual modulus of elasticity (86%). Beyond 300 °C, the 0S-0G concrete presented a 25% difference with respect to the 0S-100G concrete, and beyond 600 °C, a difference of only 9% was observed. Beyond 450 and 600 °C, the values of the three formulations differ less because of the appearance of cracks between the cement paste and coarse aggregates.

The faster degradation in RACs was likely caused by the presence of combustible waste such as bitumen, which was found in the specimens, and by the instability of the flints, which could be attributed to the recycled aggregates.

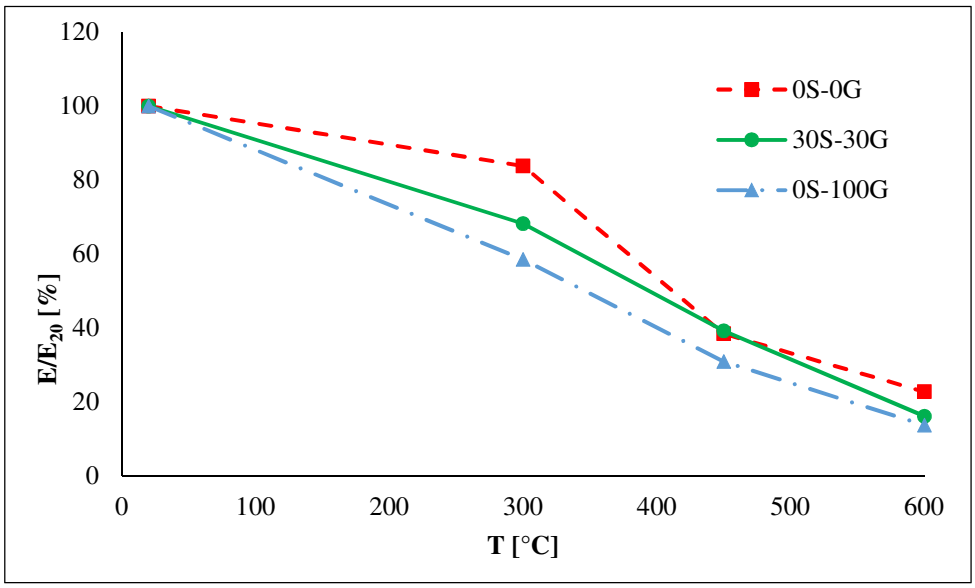

Figure 13 Relative residual dynamic moduli of elasticity for 0S-0G, 30S-30G, and 0S-100G concretes as functions of temperature

3.4 Thermal deformation properties of mortars

The preparation of mortars was necessary to analyse aggregate shrinkage/expansion. Figure 14 depicts the evolution of the dilatometry tests results for the 0S, 30S, 70S, and 100S mortars during the heating–cooling period.

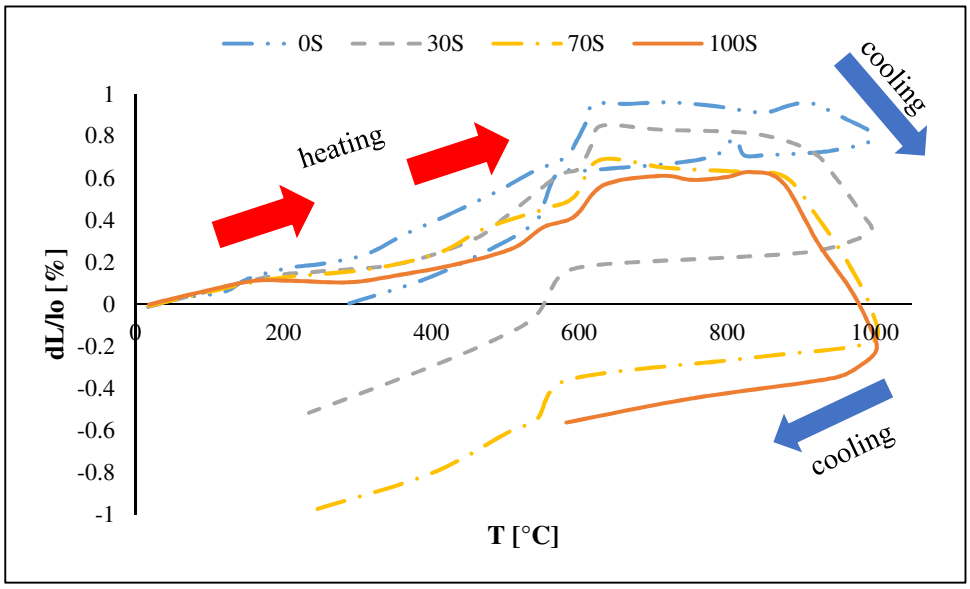

All the mortars expanded during the heating phase and shrunk during the cooling phase. The expansion amplitude decreased with the replacement of natural sand by recycled sand.

The dilatometry tests indicated the same trend up to 200 °C, as the dilatation decelerated as much as the percentage of recycled sand. Starting from this temperature, the cement paste exhibited shrinkage owing to dehydration [52]. The higher the proportion of recycled sand, the higher is the proportion of cement paste, as compared with the aggregates that expanded. Thus, the thermal expansion of the recycled sand mortar was reduced owing to the effect of the old paste cement. The dilatation evolved up to 620 °C, while the thermal expansion was less pronounced up to 900 °C. During the heating and cooling phases, the concretes exhibited progressive shrinkage between 900 and 1000 °C and from 1000 to 540 °C, respectively. From 540 to 200 °C, the shrinkage was more evident. Notably, the shrinkage increased with an increase in the percentage of recycled sand.

Figure 14 Dilatometry test results for 0S, 30S, 70S, and 100S mortars during heating–cooling period

Figure 15 depicts the thermal expansion coefficients for all the tested mortars during the heating phase. The thermal expansion coefficient of natural sand mortar (0S) was higher than those of the recycled sand mortars. The natural sand used in this study was semi-crushed, siliceous–calcareous

sand. According to Niry et al. [40], siliceous aggregates feature a high thermal expansion coefficient in the range of $\alpha = 40 \times 10^{-6}$/°C. Recycled sand includes not only siliceous recycled aggregates but also recycled cementitious pastes. Therefore, the proportion of siliceous aggregates decreased with an increase in the volume of the recycled aggregates. This is consistent with the trend in evolution of the curve with respect to the amplitude.

An increase of thermal expansion coefficient was observed at approximately 600 °C. This peak decreased with the increase of recycled aggregates. After the quartz phase change at 573 °C, the thermal expansion coefficient increased significantly [53]. The higher values of the thermal expansion coefficient lay between 590 and 620 °C (α max $_{0S} = 19.0 \times 10^{-6}$/°C, α max $_{30S} = 17.8 \times 10^{-6}$/°C, α max $_{70S} = 13.0 \times 10^{-6}$/°C, and α max $_{100S} = 11.4 \times 10^{-6}$/°C). The phase change involved an increase of 1% in the volume. This transformation was accompanied by significant specimen cracking [54].

These results were consistent with the statistical cracking analysis (Section 3.1.3), which indicated the dense cracking of concretes including siliceous aggregates beyond 600 °C.

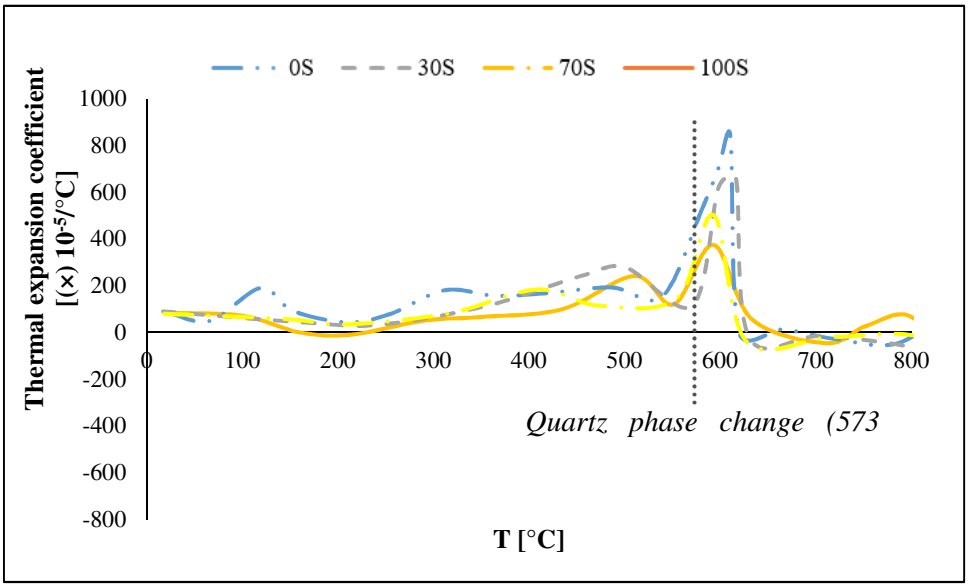

Figure 15 Thermal expansion coefficient of 0S, 30S, 70S, and 100S mortars during the heating period

4. Discussion

The objective of this study was to contribute experimentally toward a better understanding of the behaviour of RACs subjected to elevated temperatures. Concretes with natural and/or recycled aggregates were prepared, cured, and subjected to a heating rate of 0.5 °C/min. Mortars containing

natural and/or recycled sand were tested during the heating (from 20 to 1000 °C) and cooling periods (from 1000 to 200 °C).

Concretes

Measurements of the thermal properties indicated lower thermal conductivities of the 30S-30G and 0S-100G concretes at room temperature. The presence of recycled aggregates does not alter the values of specific heat. During heating, the thermal conductivities of the concretes decreased, whereas their specific heats increased slightly. Therefore, the decrease in thermal diffusivity with temperature was more pronounced, as compared with that in thermal conductivity. The trends in the evolution of thermal conductivity and specific heat of the concretes with or without recycled aggregates as a function of temperature were generally identical. Thus the diffusivity also presented a little difference between the three concretes (0S-0G, 30S-30G, and 0S-100G).

The thermal conductivity measurements during the cooling period indicated hysteresis. This hysteresis suggested the irreversibility of the reaction, which led to material damage. The presence of recycled aggregates has little effect on the specific heat. During heating, the thermal conductivity of the concrete decreases while its specific heat increases slightly. Consequently, the decrease in diffusivity with temperature is more pronounced than that of conductivity.After 500°C, the specific heat of the 0S-100G concrete exhibited a drastic surge. It corroborates the results of total porosity: this increase in the specific heat was more likely caused by the increase of the porosity within the cement paste. As the specific heat of air is lightly higher than that of concrete (Cp air = 1005 J kg^{-1} K^{-1} and Cp concrete ≈ 880 J kg^{-1} K^{-1}).

Surface, quarter, and mid-diameter temperature measurements during heating facilitated a comparison of the thermal responses of the three types of concrete (0S-0G, 30S-30G, and 0S-100G), including the amount of heat consumed during phase changes and chemical transformations. The temperature difference between the surface and the centre of the specimen was slightly higher in the concretes containing recycled aggregates (30S-30G and 0S-100G), particularly in the 30S-30G concrete. This could be attributed to the large quantity of water absorbed by the recycled sand. In general, the 30S-30G and 0S-100G concretes exhibited thermal behaviour highly similar to that of the 0S-0G concrete with lower thermal conductivity.

In terms of all the residual properties, the performance of the RACs was inferior to that of natural aggregate concrete. The residual water porosity indicated that increasing the quantity of recycled aggregates increased the values of porosity. This was attributed to the presence of the multiple ITZs (paste/natural aggregate and old paste/new paste). The results of the statistical cracking analysis were consistent with the trend in the evolution of porosity. The rate of increase in cracks grew with an increase in temperature. This was caused by presence of flints in the original aggregates of RCA, which increased in volume during heating [40,55]. Moreover, the cracks grew with an increase in the

size of the aggregates. Beyond 600 °C, 0S-100G concrete illustrated almost triple the lengths of cracks as compared with 0S-0G concretes. These results were in accordance with the residual mechanical properties. The faster degradation of RACs is also promoted by the presence of combustible wastes such as bitumen, which was found in the specimens.

Mortars

Up to 180°C, the behaviour of all mortars is identical, with the double expansion of the aggregates and the cementitious paste. Beyond this point, the dehydration of the hydrates in the cement paste induces a contraction of the cement paste while the siliceous aggregates continue to expand. The relative fraction of cement paste to alluvial sand increases with the substitution rate of recycled sand. Thus the overall expansion of the mortar decreases with the percentage of recycled sand substitution. The proportion of the "old" "contracting" cementitious paste in the recycled sand reduces the relative influence of the expansion of the siliceous minerals. Similarly at 573°C, the range of the sudden increase in thermal deformation, induced by the allotropic transformation of quartz, is more attenuated for the recycled sand mortar.

On the contrary, the higher the substitution rate, the more the mortar undergoes a significant contraction beyond 800°C. The residual deformation is dilatant for an alluvial sand mortar and contracting for a recycled sand mortar.

5. Conclusion

In this study, the effect of recycled aggregates on the thermal properties of concretes and their residual behaviour was investigated. The following conclusions were drawn based on the results:

- The thermal conductivity values of the RACs (30S-30G and 0S-100G) were lower than that of the natural aggregate concrete (0S-0G). This difference can be explained by the higher porosity and paste volume of recycled concretes. The thermal conductivity of the 0S-0G concretes decreased more rapidly, although the values of thermal conductivity for all the concretes were almost similar at 600 °C. The hysteresis that appeared during the cooling phase indicated irreversible material degradation.
- The thermal response of the three types of concrete showed a slightly higher maximum temperature difference for the concretes containing recycled aggregates, particularly for the C 30R-30R concrete, due to the higher amount of water absorbed by the recycled sand. In the light of all these results, the thermo-physical behavior of concretes C0R-100R and C30R-30R are very close to that of 0R-0R, but with lower thermal conductivities.

- The residual water porosity and mechanical properties were in accordance with the statistical cracking analysis. Above 300 °C, the residual strength and Young modulus of the RAC was slightly lower than that of the reference concrete manufactured with calcareous aggregate.
- For almost the same volume of recycled aggregate, C30R-30R concrete has less loss of strength with temperature and less cracks than C0R-100R concrete. The recycled coarse aggregate have a more unfavourable influence than the recycled sand on the residual properties. This can be explained by the mineralogical nature of the original natural aggregate of the RCAs. The analysis of the cracking of the concrete after heating shows intra-granular cracks in the original natural aggregate of the RCAs. The original natural aggregates of the RCA are alluvial aggregates consisting of 70% flint. This cryptocrystalline form of quartz is highly unstable at high temperatures. Its influence on the thermal cracking of concrete is all the more important when the aggregates are large.
- From 200 °C, the coefficient of thermal expansion of a mortar decreases with increasing percentage replacement of siliceous sand by recycled sand. This was explained by a higher proportion of contracting paste compared to the "expanding" aggregate fraction. Then, above 850 °C an additional contraction is to be noticed for the recycled sand due to a possible decarbonation of the old cementitious paste contained in the recycled sand.

6. Bibliography

[1] L. Evangelista, J. de Brito, Mechanical behaviour of concrete made with fine recycled concrete aggregates, Cem. Concr. Compos. 29 (2007) 397–401. doi:10.1016/j.cemconcomp.2006.12.004.

[2] J.M. Khatib, Properties of concrete incorporating fine recycled aggregate, Cem. Concr. Res. 35 (2005) 763–769. doi:10.1016/J.CEMCONRES.2004.06.017.

[3] X. Li, Recycling and reuse of waste concrete in China: Part II. Structural behaviour of recycled aggregate concrete and engineering applications, Resour. Conserv. Recycl. 53 (2009) 107–112. doi:10.1016/J.RESCONREC.2008.11.005.

[4] R.K. Dhir, M.C. Limbachiya, T. Leelawat, Suitability of recycled concrete aggregate for use in bs 5328 designated mixes, Proc. Inst. Civ. Eng. 134 (1999).

[5] M. Breccolotti, A.L. Materazzi, Structural reliability of eccentrically-loaded sections in RC columns made of recycled aggregate concrete, Eng. Struct. 32 (2010) 3704–3712. doi:10.1016/J.ENGSTRUCT.2010.08.015.

[6] NTC - 2008, Norme techniche per le construczioni (Italian recommendations), 29 Decreto Minist. 14 Gennaio. (28AD).

[7] RILEM-TC-121-DRG, Specifications for concrete with recycled aggregates, 1994.

[8] Y. Zaetang, V. Sata, A. Wongsa, P. Chindaprasirt, Properties of pervious concrete containing recycled concrete block aggregate and recycled concrete aggregate, Constr. Build. Mater. 111 (2016) 15–21. doi:10.1016/J.CONBUILDMAT.2016.02.060.

[9] S.-W. Kim, H.-D. Yun, W.-S. Park, Y.-I. Jang, Bond strength prediction for deformed steel rebar embedded in recycled coarse aggregate concrete, Mater. Des. 83 (2015) 257–269. doi:10.1016/J.MATDES.2015.06.008.

[10] M.P. Adams, T. Fu, A.G. Cabrera, M. Morales, J.H. Ideker, O.B. Isgor, Cracking susceptibility of concrete made with coarse recycled concrete aggregates, Constr. Build. Mater. 102 (2016) 802–810. doi:10.1016/J.CONBUILDMAT.2015.11.022.

[11] S.W. Tabsh, A.S. Abdelfatah, Influence of recycled concrete aggregates on strength properties

of concrete, Constr. Build. Mater. 23 (2009) 1163–1167. doi:10.1016/J.CONBUILDMAT.2008.06.007.

[12] W.H. Kwan, M. Ramli, K.J. Kam, M.Z. Sulieman, Influence of the amount of recycled coarse aggregate in concrete design and durability properties, Constr. Build. Mater. 26 (2012) 565–573. doi:10.1016/j.conbuildmat.2011.06.059.

[13] Z.H. Duan, C.S. Poon, Properties of recycled aggregate concrete made with recycled aggregates with different amounts of old adhered mortars, Mater. Des. 58 (2014) 19–29. doi:10.1016/J.MATDES.2014.01.044.

[14] Z. Xiao, W.G. Li, Z.H. Sun, S.P. Shah, Crack Propagation in Recycled Aggregate Concrete under Uniaxial Compressive Loading, ACI Mater. J. (2012) 451–461.

[15] M.J. McGinnis, M. Davis, A. de la Rosa, B.D. Weldon, Y.C. Kurama, Strength and stiffness of concrete with recycled concrete aggregates, Constr. Build. Mater. 154 (2017) 258–269. doi:10.1016/j.conbuildmat.2017.07.015.

[16] T.C. Hansen, Recycled aggregates and recycled aggregate concrete second state-of-the-art report developments 1945-1985, Mater. Struct. 19 (1986) 201–246. doi:10.1007/BF02472036.

[17] D. Cree, M. Green, A. Noumowé, Residual strength of concrete containing recycled materials after exposure to fire: A review, Constr. Build. Mater. 45 (2013) 208–223. doi:10.1016/J.CONBUILDMAT.2013.04.005.

[18] Y. Guo, J. Zhang, G. Chen, Z. Xie, Compressive behaviour of concrete structures incorporating recycled concrete aggregates, rubber crumb and reinforced with steel fi bre , subjected to elevated temperatures, J. Clean. Prod. 72 (2014) 193–203. doi:10.1016/j.jclepro.2014.02.036.

[19] E. Meng, Y. Yu, J. Yuan, K. Qiao, Y. Su, Triaxial compressive strength experiment study of recycled aggregate concrete after high temperatures, Constr. Build. Mater. 155 (2017) 542–549. doi:10.1016/j.conbuildmat.2017.08.101.

[20] F.B. Varona, F. Baeza-Brotons, A.J. Tenza-Abril, F.J. Baeza, L. Bañón, Residual compressive strength of recycled aggregate concretes after high temperature exposure, Materials (Basel). 13 (2020). doi:10.3390/MA13081981.

[21] H. Yang, Y. Qin, Y. Liao, W. Chen, Shear behavior of recycled aggregate concrete after exposure to high temperatures, Constr. Build. Mater. 106 (2016) 374–381. doi:10.1016/j.conbuildmat.2015.12.103.

[22] C.J. Zega, A. Antonio, D. Maio, Recycled concrete made with different natural coarse aggregates exposed to high temperature, Constr. Build. Mater. 23 (2009) 2047–2052. doi:10.1016/j.conbuildmat.2008.08.017.

[23] R. Jansson, L. Boström, Spalling of concrete exposed to fire (SP Report 2008:52), 2008.

[24] K. Hertz, Limits of Spalling of Fire-Exposed Concrete, Fire Saf. J. 38. (2003).

[25] S.C. Kou, C.S. Poon, M. Etxeberria, Residue strength, water absorption and pore size distributions of recycled aggregate concrete after exposure to elevated temperatures, Cem. Concr. Compos. 53 (2014) 73–82. doi:10.1016/j.cemconcomp.2014.06.001.

[26] Y. Wang, F. Liu, L. Xu, H. Zhao, Effect of elevated temperatures and cooling methods on strength of concrete made with coarse and fine recycled concrete aggregates, Constr. Build. Mater. 210 (2019) 540–547. doi:10.1016/j.conbuildmat.2019.03.215.

[27] C. Laneyrie, A. Beaucour, M.F. Green, R.L. Hebert, B. Ledesert, A. Noumowe, Influence of recycled coarse aggregates on normal and high performance concrete subjected to elevated temperatures, 111 (2016) 368–378. doi:10.1016/j.conbuildmat.2016.02.056.

[28] D. Xuan, B. Zhan, C.S. Poon, Thermal and residual mechanical profile of recycled aggregate concrete prepared with carbonated concrete aggregates after exposure to elevated temperatures, Fire Mater. 42 (2018) 134–142. doi:10.1002/fam.2465.

[29] J. Xie, Z. Zhang, Z. Lu, M. Sun, Coupling effects of silica fume and steel-fiber on the compressive behaviour of recycled aggregate concrete after exposure to elevated temperature, Constr. Build. Mater. 184 (2018) 752–764. doi:10.1016/j.conbuildmat.2018.07.035.

[30] National Project Recybeton report n° R/13/RECY/003, in French, 2017.

[31] EUROCODE 2, Design of concrete structures – Part 1-2: General rules – structural fire design, TC 250. (2004).

[32] NF EN 109-6 AFNOR, Tests for mechanical and physical properties of aggregates - Part 6: Determination of particle density and water absorption, (2001).

[33] F. De Larrard, Concrete Mixture Proportioning, CRC Press, London, 1999. doi:10.1201/9781482272055.

[34] 200-HTC Recommendation of RILEM TC, Mechanical concrete properties at high temperatures—modelling and application, Mater. Struct. 40 (2007) 449–458. doi:10.1617/s11527-006-9203-z.

[35] AFNOR, Concrete - Testing hardened concrete - Testing porosity and density, NF P 18-459. (2010).

[36] AFNOR, Testing hardened concrete. Compressive strength of test specimens, NF EN 12390-3. (2003).

[37] NF EN 12504-4, Essais pour béton dans les structures - Partie 4 : determination de la vitesse de

propagation du son., (2005).

[38] S.E. Gustafsson, Transient plane source techniques for thermal conductivity and thermal diffusivity measurements of solid materials, Rev. Sci. Instrum. 63 (1991) 797–804.

[39] T. Gustafsson S.E., Long, Transient plane source (TPS) technique for measuring thermal transport properties of building materials, Fire Mater. 19 (1995) 43–49.

[40] R. Niry, A. Beaucour, R.L. Hebert, B. Ledesert, R. Bodet, A. Noumowe, High temperature behaviour of a wide petrographic range of siliceous and calcareous aggregates for concretes, Constr. Build. Mater. 123 (2016) 261–273. doi:10.1016/j.conbuildmat.2016.06.097.

[41] H. Zhao, Thermal properties of coarse RCA concrete at elevated temperatures, Appl. Therm. Eng. 140 (2018) 180–189. doi:10.1016/j.applthermaleng.2018.05.032.

[42] Z. Xing, A.-L. Beaucour, R. Hebert, A. Noumowe, B. Ledesert, Aggregate's influence on thermophysical concrete properties at elevated temperature, Constr. Build. Mater. 95 (2015) 18–28.

[43] R. Niry Razafinjato, A.-L. Beaucour, R. Hébert, A. Noumowé, R. Bodet, Comportement à haute température des bétons de granulats naturels siliceux et calcaires, Rencontres Univ. AUGC. (2014) 1–11.

[44] N. Yermak, P. Pliya, A. Beaucour, A. Simon, A. Noumowé, Influence of steel and / or polypropylene fibres on the behaviour of concrete at high temperature : Spalling , transfer and mechanical properties, Constr. Build. Mater. 10 (2017) 240–250. doi:10.1016/j.conbuildmat.2016.11.120.

[45] R. Jansson, Material properties related to fire spalling of concrete, Report, Lund Institute of technology, 2004.

[46] P. Pliya, H. Hajiloo, S. Romagnosi, D. Cree, S. Sarhat, M.F. Green, The compressive behaviour of natural and recycled aggregate concrete during and after exposure to elevated temperatures, J. Build. Eng. 38 (2021) 102214. doi:10.1016/j.jobe.2021.102214.

[47] C. Thomas, J. Setién, J.A. Polanco, J. de Brito, F. Fiol, Micro- and macro-porosity of dry- and saturated-state recycled aggregate concrete, J. Clean. Prod. 211 (2019) 932–940. doi:10.1016/J.JCLEPRO.2018.11.243.

[48] P. Pliya, D. Cree, H. Hajiloo, A.L. Beaucour, M.F. Green, A. Noumowé, High-Strength Concrete Containing Recycled Coarse Aggregate Subjected to Elevated Temperatures, Fire Technol. 55 (2019) 1477–1494. doi:10.1007/s10694-019-00820-0.

[49] Z. Xing, R. Hebert, A.-L. Beaucour, B. Ledesert, A. Noumowe, Influence of chemical and mineralogical composition of concrete aggregates on their behaviour at elevated temperature,

Mater. Struct. 47 (2014) 1921–1940.

[50] G. Dreux, J. Festa, New guide of concretes and its components, eigth edition, Ed. Eyrolles. (2002).

[51] T. Xie, A. Gholampour, T. Ozbakkaloglu, Toward the Development of Sustainable Concretes with Recycled Concrete Aggregates: Comprehensive Review of Studies on Mechanical Properties, J. Mater. Civ. Eng. 30 (2018) 04018211. doi:10.1061/(ASCE)MT.1943-5533.0002304.

[52] W. Khaliq, Taimur, Mechanical and physical response of recycled aggregates high-strength concrete at elevated temperatures, Fire Saf. J. 96 (2018) 203–214. doi:10.1016/J.FIRESAF.2018.01.009.

[53] C.J. Zega, A.A. Di Maio, Recycled concrete made with different natural coarse aggregates exposed to high temperature, Constr. Build. Mater. 23 (2009) 2047–2052. doi:10.1016/J.CONBUILDMAT.2008.08.017.

[54] I. Hager, Comportement à haute température des bétons à haute performance - évolution des principales propriétés mécaniques, Thèse de doctorat, Ecole Nationale des Ponts et Chaussées et l'Ecole Polytechnique de Cracovie, 2004.

[55] Z. Xing, A.-L. Beaucour, R. Hebert, A. Noumowé, B. Ledesert, Influence of the nature of aggregates on the behaviour of concrete subjected to elevated temperature, Cem. Concr. Res. 41 (2011) 392–402. doi:10.1016/j.cemconres.2011.01.005.